Journal of Molecular Medicine
https://doi.org/10.1007/s00109-023-02328-1

JMolMed

ORIGINAL ARTICLE

LAMP2A regulates the balance of mesenchymal stem cell adipo-osteogenesis via the Wnt/β-catenin/GSK3β signaling pathway

Yibo Wang[1,2] · Kai Hang[1,2] · Li Ying[3] · Jiaqi Wu[1,2] · Xiaoyong Wu[1,2] · Weijun Zhang[1,2] · Lijun Li[1,2] · Zhongxiang Wang[1,2] · Jinwu Bai[1,2] · Xiang Gao[1,2] · Deting Xue[1,2] · Zhijun Pan[1,2]

Received: 19 October 2022 / Revised: 24 April 2023 / Accepted: 25 April 2023

Abstract

Chaperone-mediated autophagy (CMA) plays multiple roles in cell metabolism. We found that lysosome-associated membrane protein type 2A (LAMP2A), a crucial protein of CMA, plays a key role in the control of mesenchymal stem cell (MSC) adipo-osteogenesis. We identified a differentially expressed CMA gene (LAMP2) in GEO datasets (GSE4911 and GSE494). Further, we performed co-expression analyses to define the relationships between CMA components genes and other relevant genes including Col1a1, Runx2, Wnt3 and Gsk3β. Mouse BMSCs (mMSCs) exhibiting Lamp2a gene knockdown (LA-KD) and overexpression (LA-OE) were created using an adenovirus system; then we investigated LAMP2A function in vitro by Western blot, Oil Red staining, ALP staining, ARS staining and Immunofluorescence analysis. Next, we used a modified mouse model of tibial fracture to investigate LAMP2A function in vivo. LAMP2A knockdown in mMSCs decreased the levels of osteogenic-specific proteins (COL1A1 and RUNX2) and increased those of the adipogenesis markers PPARγ and C/EBPα; LAMP2A overexpression had the opposite effects. The active-β-catenin and phospho-GSK3β (Ser9) levels were upregulated by LAMP2A overexpression and downregulated by LAMP2A knockdown. In the mouse model of tibial fracture, mMSC-overexpressing LAMP2A improved bone healing, as demonstrated by microcomputed tomography and histological analyses. In summary, LAMP2A positively regulates mMSC osteogenesis and suppresses adipo-osteogenesis, probably via Wnt/β-catenin/GSK3β signaling. LAMP2A promoted fracture-healing in the mouse model of tibial fracture.

Key messages

- LAMP2 positively regulates the mBMSCs osteogenic differentiation.
- LAMP2 negatively regulates the mBMSCs adipogenic differentiation.
- LAMP2 regulates mBMSCs osteogenesis via Wnt/β-catenin/GSK3β signaling pathway.
- LAMP2 overexpression mBMSCs promote the fracture healing.

Keywords CMA · LAMP2A · mMSCs · Osteogenesis · Adipogenesis · Wnt/β-catenin/GSK3β

Introduction

Fractures are the most common musculoskeletal injuries in the United States (approximately 5 million in 2017) [1]. Despite improvements in treatment, around 4.9% of patients exhibit delayed healing or nonunion [2]. Fractures impose major societal and healthcare burdens [3, 4]. Thus, more effective treatments are required. Fracture healing can be divided into inflammation, callus formation, and remodeling [5]. After hematoma formation, inflammatory factors recruit

Yibo Wang, Kai Hang, and Li Ying are authors contributed equally to this work.

✉ Xiang Gao
gaoxiang162@zju.edu.cn

✉ Deting Xue
blueskine@zju.edu.cn

✉ Zhijun Pan
zrpzj@zju.edu.cn

[1] Department of Orthopedic Surgery of the Second Affiliated Hospital, School of Medicine, Zhejiang University, No. 88, Jiefang Road, Hangzhou 310009, China

[2] Orthopedics Research Institute of Zhejiang University, No. 88, Jiefang Road, Hangzhou 310009, China

[3] Department of Orthopedic, Taizhou Hospital of Zhejiang Province, Wenzhou Medical University, No. 150, Ximen Street, Linhai 317000, China

Published online: 10 May 2023

functional cells such as mesenchymal stem cells (MSCs), skeletal stem cells, and vascular progenitor cells to the fracture site, forming new bone on newly formed cartilage [6]. MSCs can engage in osteogenesis, adipogenesis, and chondrogenesis, greatly aiding the healing of nonunion fractures and osteogenesis imperfecta [7]. In the bone marrow, MSC osteogenesis and adipogenesis are in delicate balance. Several studies have shown that, in osteoporosis, MSCs engage principally in adipogenesis rather than osteogenesis, triggering bone marrow lipid accumulation and bone mass reduction [8–10].

Chaperone-mediated autophagy (CMA) triggers the lysosomal degradation of soluble cytosolic proteins [11]. The KFERQ motif is recognized by lysosome-targeting proteins such as heat shock protein A8 (HSPA8); proteins are translocated into lysosomes after binding to HSPA8 and the receptor protein lysosome-associated membrane protein type 2A (LAMP2A), and then are completely degraded [11–13]. The rate-limiting step of CMA is the binding of the chaperone complex to LAMP2A [14] and changes in LAMP2A levels modulate the activity [15]. LAMP2 deficiency accelerates the progression of diseases of aging, including basal retinal laminar deposition [16] and Parkinson's disease [17]. Danon's disease (an X-linked disorder characterized by hypertrophic cardiomyopathy, myopathy, and intellectual disability) is caused by an LAMP2 deficiency [18, 19]. Bone marrow stem cell infusion upregulates LAMP2 in β cells and protects the cells from injury induced by chronically high glucose levels [20]. In terms of bone formation, coculture of osteoclast precursors and LAMP2- deficient osteoblasts yield almost no osteoclasts, indicating that (osteogenic) LAMP2 is indispensable for osteoclast differentiation [21]. Previous study indicated that LAMP2A is involved in osteogenic cell lines mineralization after stimulated with ascorbic acid and phosphate (Pi) [22]. Moreover, LAMP2A and LAMP2C global knockout mice have low vertebral cancellous bone mass. LAMP2A knockdown of an osteoblastic UAMS-32 cell line decreases mineral deposition [23]. These studies indicated that LAMP2A is relative to bone formation. However, the effect of LAMP2A on mMSC differentiation and function remains unclear. Thus, we explored LAMP2A function in the context of the MSC osteogenesis/adipogenesis balance.

Methods and materials

Differentially expressed gene analyses and bioinformatics analyses

The gene expression databases of mice wildtype and RUNX2 knockout humeri (GSE4911-GPL83), human non-union skeletal fracture samples and normal samples (GSE494-GPL92) were downloaded from Gene Expression Omnibus (GEO) datasets. The differentially expressed genes (DEGs) were kept when $|\log FC| > 1$ and adj.P.Value < 0.05. The calculations were performed by R and R studio software (version 4.0.2), using the R package "limma" [24]. Next, selected genes were estimated the functional enrichments, including Kyoto Encyclopedia of Genes and Genomes (KEGG) pathways and Gene Ontology (GO) terms, using the Database for Annotation, Visualization and Integrated Discovery (DAVID) website (https://david.ncifcrf.gov/).

Cell culture and differentiation

mBMSCs were purchased from Cyagen Biosciences (MUBMX-01001, Guangzhou, China). Cells cultured in an atmosphere of 5% CO2 at 37 °C in α-MEM with 10% Fetal Bovine Serum (Biological Industries, 04-010-1A, Israel). Adipogenic induction medium was purchased from Cyagen Biosciences (MUXMX-90031). Osteogenic induction medium was prepared according to previous methods [25], and the cells were maintained by changing fresh induction medium every 2 days. Recombinant DKK-1 were purchased from MedChemExpress (HY-P7154, Shanghai, China).

Adenoviral vectors

Adenovirus vectors knockdown LAMP2A(LA-KD), overexpression LAMP2A (LA-OE) and the negative control (LA-NC) were purchased from Cyagen Biosciences (Supplementary Table 1). 50-60% confluent mBMSCs were incubated with adenovirus particles at an optimal MOI and 4 μg/ml polybrene (Cyagen Biosciences). After 12 hours, the culture medium was changed and the transfected cells were used in next experiments.

Cell proliferation assay

To estimate the effect of LAMP2A knockdown and LAMP2A overexpression on mMSCs proliferation, related cells were seed into 96-wells plate. After 1-7days proliferation, the medium was changed by 10% Cell Counting Kit-8 (CCK-8, Dojindo, Kumamoto, Japan) in 100μl α-MEM for 4h at 37 °C. The absorbance at 450nm which is proportional to the living cells number, was measured by a microplate reader (ELX808, BioTek, USA).

Co-relationship analysis

The raw expression data of LAMP2, HSPA8, COL1A1, RUNX2, WNT3 and GSK3B genes were downloaded from the Cancer Cell Line Encyclopedia (CCLE) project (https://portals.broadinstitute.org/ccle), The Cancer Genome Atlas (TCGA) project (http://cancergenome.nih.gov/) and the Genotype Tissue

Expression (GTEx) project (https://www.gtexportal.org/). The Pearson correlation (R) analysis and p-value were calculated by R and R studio software (version 4.0.2).

RNA isolation and qPCR

Total RNA was isolated by RNAiso Plus (9109, Takara Bio Inc., Shiga, Japan) and quantified by measuring the absorbance at 260 nm (NanoDrop 2000, Thermo Fisher Scientific, MA, USA). First strand cDNA was synthesized by PrimeScript RT Master Mix (Takara) according to the manufacturer's instructions. Total RNA (≤ 1000 ng) was reverse-transcribed into cDNA using the Double-Strand cDNA Synthesis Kit (Takara) in a reaction volume of 20 µl. The levels of all gene expressions were quantified by qPCR using SYBR Green PCR Master Mix (Takara) on StepOnePlus real-time PCR system (Applied Biosystems Inc., Warrington, United Kingdom). The cycle conditions were as follows: 95 °C for 30s followed by 40 cycles of 95 °C for 5s and 60 °C for 30s. 18S was used as a control and allowed adjustment of differences among samples. The relative target gene expression levels were calculated using the $2-\Delta\Delta Ct$ method. Primers sequence for 3 isoforms of Lamp2 (Lamp2a, Lamp2b and Lamp2c) were acquired from previous study [26]. All primers were synthesized by Tsingke Biotechnology and listed at Supplementary Table 2.

Western blotting analysis

Cells were lysed in RIPA buffer (Fdbio Science, FD008, Hangzhou, China) mixed with proteasome inhibitor (Fdbio Science, FD1001) and phosphatase inhibitors (Fdbio Science, FD1002). Equal amounts of proteins were separated by 10% SDS-PAGE and then transferred onto polyvinylidene fluoride (PVDF) membranes (Millipore, Shanghai, China). After blocking in 5% non-fat milk for 1 h, the membranes were incubated overnight at 4 °C with antibodies specific to α-Tubulin (1:1000, AF0001, Beyotime, Shanghai, China), LAMP2A (1:1000, AF1036, Beyotime), RUNX2 (1:1000, #12556, Cell Signaling Technology, Danvers, MA, United States), COL1A1 (1:1000, ab34710, Abcam, Cambridge, United Kingdom), PPARγ (1:1000, AF7797, Beyotime), C/EBPα (1:1000, #8178, Cell Signaling Technology), non-phosphorylated (active) β-catenin (1:1000, #19807, Cell Signaling Technology), total β-catenin (1:1000, #8480, Cell Signaling Technology), GSK3β (1:1000, #12456, Cell Signaling Technology), and Phospho-GSK3β (Ser9) (1:1000, #5558, Cell Signaling Technology). After washing 3 times (10 minutes each time) in Tris-buffered saline with 0.1% Tween 20 (TBST), the membranes were incubated with horseradish peroxidase (HRP)-labeled Goat Anti-Rabbit IgG(H+L) (1:1000, A0208, Beyotime) for 1h at room temperature. After washing three times (5 minutes each time) with TBST, proteins were detected using enhanced chemiluminescence blotting reagents (Millipore). Signal intensity was measured by Bio-Rad XRS chemiluminescence detection system (Bio-Rad, Hercules, CA, USA).

ALP staining

Cells were cultured in 12-well plates with osteogenic induction medium for 5 days. For ALP staining, cells were fixed with 4% paraformaldehyde for 30 minutes. Cells were then washed by double distilled water (ddH2O) 3 times and stained by BCIP/NBT Alkaline Phosphatase Color Development Kit (C3206, Beyotime). To measure ALP activity, cells were lysed with lysis buffer consisted of 20 mM Tris-HCl (pH 7.5), 1% Triton X-100, and 150mM NaCl. ALP activity was determined by ALP activity assay (P0321S, Beyotime). Finally, the conversion color of p-nitrophenyl phosphate was measured after 5 days of culture in an osteogenic medium at 405/650nm.

Alizarin red staining

Mineral deposition was assessed by Alizarin Red staining (ARS) (Cyagen Biosciences) after the induction of osteogenic differentiation for 21 days. Cells were fixed with 4% paraformaldehyde for 30 minutes at room temperature and subsequently washed with PBS three times. The cells were incubated with a 0.2% solution of Alizarin Red for 10 minutes at room temperature, then rinsed with PBS 3 times. The stain is incubated with 10% cetylpyridinium chloride (Sigma, Shanghai, China) for 1 h and collected the solutions, then 200µl was plated on a 96-well plate and then was read at 560nm by a microplate reader (ELX808, BioTek). The results were normalized to total protein concentration.

Oil red O staining

Cells were cultured in 12-well plates with adipogenic induction medium following the protocol (Cyagen Biosciences, MUXMX-90031) for 21 days. Cells were fixed with 4% paraformaldehyde for 30 minutes at room temperature and subsequently rinsed with PBS 3 times. Cells were stained with 0.5ml of oil red O working solution for 30 minutes following the protocol (Cyagen Biosciences, MUXMX-90031). Semi-quantitative analysis was performed by ImageJ (version 1.53).

Cell immunofluorescence analysis

Cells were cultured in a 24-well plate with induction medium and evaluated for RUNX2 and COL1A1 using a fluorescence microscope (EU5888, Leica, Germany) as follows. Cells were fixed in 4% paraformaldehyde for 20 minutes at room temperature, permeabilized for 30 minutes in 0.2% Triton X-100, and blocked for 30 minutes in 2% bovine serum

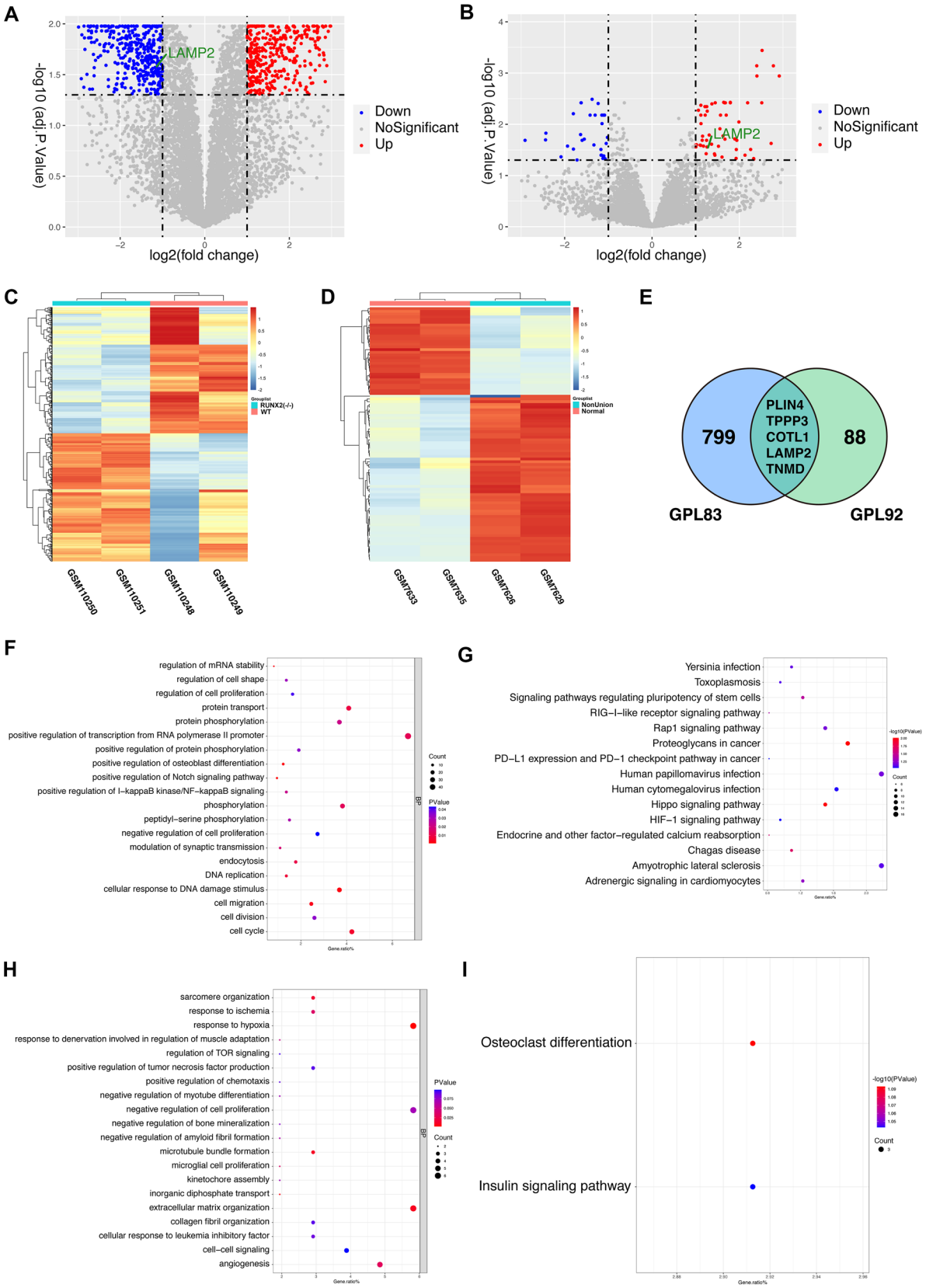
A
LAMP2
-log10 (adj.P.Value)
log2(fold change)
Down
NoSignificant
Up
B
LAMP2
-log10 (adj.P.Value)
log2(fold change)
Down
NoSignificant
Up
C
RUNX2(-/-)
WT
GSM110250
GSM110251
GSM110248
GSM110249
D
NonUnion
Normal
GSM7633
GSM7635
GSM7626
GSM7629
E
799
88
PLIN4
TPPP3
COTL1
LAMP2
TNMD
GPL83
GPL92
F
regulation of mRNA stability
regulation of cell shape
regulation of cell proliferation
protein transport
protein phosphorylation
positive regulation of transcription from RNA polymerase II promoter
positive regulation of protein phosphorylation
positive regulation of osteoblast differentiation
positive regulation of Notch signaling pathway
positive regulation of I-kappaB kinase/NF-kappaB signaling
phosphorylation
peptidyl-serine phosphorylation
negative regulation of cell proliferation
modulation of synaptic transmission
endocytosis
DNA replication
cellular response to DNA damage stimulus
cell migration
cell division
cell cycle
Count
PValue
BP
Gene.ratio%
G
Yersinia infection
Toxoplasmosis
Signaling pathways regulating pluripotency of stem cells
RIG-I-like receptor signaling pathway
Rap1 signaling pathway
Proteoglycans in cancer
PD-L1 expression and PD-1 checkpoint pathway in cancer
Human papillomavirus infection
Human cytomegalovirus infection
Hippo signaling pathway
HIF-1 signaling pathway
Endocrine and other factor-regulated calcium reabsorption
Chagas disease
Amyotrophic lateral sclerosis
Adrenergic signaling in cardiomyocytes
-log10(PValue)
Count
Gene.ratio%
H
sarcomere organization
response to ischemia
response to hypoxia
response to denervation involved in regulation of muscle adaptation
regulation of TOR signaling
positive regulation of tumor necrosis factor production
positive regulation of chemotaxis
negative regulation of myotube differentiation
negative regulation of cell proliferation
negative regulation of bone mineralization
negative regulation of amyloid fibril formation
microtubule bundle formation
microglial cell proliferation
kinetochore assembly
inorganic diphosphate transport
extracellular matrix organization
collagen fibril organization
cellular response to leukemia inhibitory factor
cell-cell signaling
angiogenesis
PValue
Count
BP
Gene.ratio%
I
Osteoclast differentiation
Insulin signaling pathway
-log10(PValue)
Count
Gene.ratio%

◂**Fig. 1** DEGs and Functional Enrichment Analyses Between Wildtype and RUNX2 Knockout Mice Humeri (GSE4911-GPL83) and Between Non-union Fracture and Normal Human Bone Samples (GSE494-GPL92). (**A**) Volcano Plots of normalized gene expressions in GSE4911-GPL83. (**B**) Volcano Plots of normalized gene expressions in GSE494-GPL92. (**C**) Heatmaps of differentially expressed genes at GSE4911-GPL83. (**D**) Heatmaps of differentially expressed genes at GSE494-GPL92. (**E**) Venn plot show 5 differentially expressed genes, including LAMP2, at the intersection of these two databases. (**F**-**G**) The functional enrichment analyses, KEGG and GO, of the differentially expressed genes in GSE4911-GPL83. (**H**- **I**) The functional enrichment analyses, KEGG and GO, of the differentially expressed genes in GSE494-GPL92. |logFC| > 1 and adj.P.Value < 0.05

albumin. Fixed cells were washed with ddH2O three times and incubated overnight with anti-RUNX2 (1:2000, #12556, Cell Signaling Technology) or anti-COL1A1 (1:500, 67288-1-Ig, Proteintech, Wuhan, Hubei, China). After washing three times with ddH2O, cells were incubated with Alexa Fluor 555-labeled Donkey Anti-Rabbit IgG(H+L) (1:500, A0453, Beyotime) and Cy3-labeled Goat Anti-Mouse IgG(H+L) (1:500, A0521, Beyotime), respectively, for 1h at room temperature. The nuclei were stained with 4′,6-diamidino-2-phenylindole (DAPI) (10μg/ml, C1002, Beyotime) for 5 minutes. Target proteins were observed under a fluorescence microscope (Leica, Germany). Semi-quantitative analysis was performed by ImageJ (version 1.53).

Mice tibial fracture model

Mice tibial fracture model was modified based on the previous method [27]. Briefly, mice anesthetized by intraperitoneally injection of 0.3% pentobarbital sodium (30mg/kg). Exposed the right lower limb, made an incision lateral between the middle of tibial tuberosity and crest. A 0.38-mm diameter intramedullary fixation pin was then inserted into the tibial medullary canal at the level of the tibial tuberosity for fixation. Separated the soft tissue carefully and stripped the periosteum above the crest of tibia. Then an osteotomy was created about 0.5cm distal to the tibial platform. The same leg was used in each group.

For in vivo study of LAMP2A overexpression effects, mice were divided into 3 groups, blank group (BLANL), negative control (LA-NC) group and LAMP2A overexpression (LA-OE) group. 20μl PBS, 5×10^6 LA-NC mMSCs and 5×10^6 LA-OE mMSCs was injected into fracture site locally, respectively. 4 weeks after surgery, limbs were harvested after lethal intraperitoneal injection of 0.1 ml sodium pentobarbitone (200 mg/ml) for next experiments.

MicroCT analysis

Following harvest, specimens were sent to make a micro-computed tomography (microCT) evaluation. Each tibia was scanned using MILabs microCT system (Utrecht, Netherlands), and operation parameters were using according to the previous report [28]. The BV (bone volume), BV/TV (bone volume fraction), Tb.Th (trabecular thickness) and Tb.Sp (trabecular separation) were evaluated by three-dimensional standard microstructural analysis [29] using Imalytics Preclinical system (version 2.1.8.9) [30]. The microCT analysis were performed 0.5cm around the fracture area.

Histology and immunohistochemistry (IHC)

Following harvest, samples were fixed by 10% paraformaldehyde for 36 hours at 4 °C and then were decalcified by 0.5M ethylene diaminetetra acetic acid (EDTA, Beyotime) for 3 days at 4 °C. Specimens were then embedded in paraffin and sectioned at a 5um thickness. Serial sections were deparaffinized and then stained with Hematoxylin-Eosin (H&E) staining, Safranin O/Fast Green staining and Masson's Trichrome staining following the standard procedures. As for IHC, 5 mm sections of paraffin-embedded tissues were deparaffinized and repaired in Trypsin Digestion Solution, 0.1% (X1020, Solarbio, Beijing, China) at 37 °C for 1 hour. Then, Immunostaining was performed using an IHC kit (ZSGB-BIO, SP-9001, Wuxi, Jiangsu, China) according to the procedure. A rabbit monoclonal anti-osteopontin (OPN) (1:1000, ab214050, Abcam) was used to detect the OPN positive cells at the bone fracture healing area. Finally, DAB substrate kit (DA1016, Solarbio) was used to coloration and Mayer's Hematoxylin solution (G1080, Solarbio) was used to color the cell nucleus.

Histological immunofluorescence analysis

After deparaffinized and repaired, sections were permeabilized with 0.3% Triton X-100 at room temperature for 10 minutes and blocked in 3% bovine serum albumin for 1 hour. Then, sections were incubated at 4 °C with primary antibodies overnight. The following primary antibodies were used: anti-ALP (1:200, #DF6225, Affinity Biosciences). After that, sections were incubated with fluorescent secondary antibody, Alexa Fluor 555-labeled Donkey Anti-Rabbit IgG(H+L) (1:500, A0453, Beyotime). After stained the nuclei with DAPI (10μg/ml, C1002, Beyotime) for 5 minutes, sections were observed under a fluorescence microscope (Leica, Germany).

Statistical analysis

All statistical analyses were performed using GraphPad Prism (version 8.2.0, GraphPad Software, San Diego, CA, United States). All experiments were conducted at least three

times and the data are presented as means ± SD. One-way analysis of variance (ANOVA) followed by Dunnett's multiple comparisons test was used to compared the data involves multiple group comparisons. In all analyses, $p < 0.05$ was taken to indicate statistical significance.

Results

LAMP2 is a bone formation relative gene

To investigate the possible bone formation relative genes, we performed differentially expressed gene analyses on Gene Expression Omnibus (GEO) datasets. Through setting a threshold of |logFC| > 1 and adj.P.Value < 0.05, 804 differentially expressed genes were identified from the database of mice wildtype and RUNX2 knockout humeri(GSE4911-GPL83) (Fig. 1A, C) and 93 differentially expressed genes were identified from the database of human non-union skeletal fracture samples and normal samples (GSE494-GPL92) (Fig. 1B, D). When we intersected these results, interestingly, 5 common differentially expressed genes were obtained (Fig. 1E). Furthermore, we analyzed the top 20 enriched signaling by GO terms (BP for Biological Process) of GSE4911-GPL83 and GSE494-GPL92, respectively. DEGs in GSE4911-GPL83 might be involved in osteoblast differentiation protein transport, protein phosphorylation and cell proliferation (Fig. 1I). Thus, we predicted that LAMP2 is a bone formation relative gene.

Endogenous LAMP2A expression increases during mMSC osteogenesis

We measured endogenous LAMP2A expression levels during mMSC osteogenic differentiation. The LAMP2A protein level increased as the concentrations of osteogenesis markers (including COL1A1 and RUNX2) increased from day 0 to 28 (Fig. 2A-D).

LAMP2A favors mMSC osteogenesis rather than adipogenesis

To explore whether CMA plays a role in osteogenesis, we assessed potential correlations between LAMP2, HSPA8, COL1A1, and RUNX2 levels (Supplementary Table 3). The Cancer Cell Line Encyclopedia (CCLE) database revealed that, in 968 cancer cell lines, the LAMP2 levels exhibited significant positive correlations with those of both COL1A1 ($R = 0.36$, $p < 0.001$) and RUNX2 ($R = 0.38$, $p < 0.001$) (Fig. 3A-B). The HSPA8 levels correlated positively with those of COL1A1 ($R = 0.12$, $p < 0.001$) but not RUNX2 ($R = 0.01$, $p = 0.800$) (Fig. 3C-D). In 93 osseous and chondromatous neoplasms and miscellaneous bone tumors of the Cancer Genome Atlas (TCGA) project, LAMP2 levels correlated positively with those of COL1A1 ($R = 0.46$, $p < 0.001$) and RUNX2 ($R = 0.51$, $p < 0.001$) (Fig. 3E-F). However, no significant correlations were evident between the HSPA8 and COL1A1 levels ($R = 0.12$, $p = 0.230$) but the levels of HSPA8 and RUNX2 were positively correlated ($R = 0.30$, $p = 0.003$) (Fig. 3G-H). In the 17,382 normal tissues

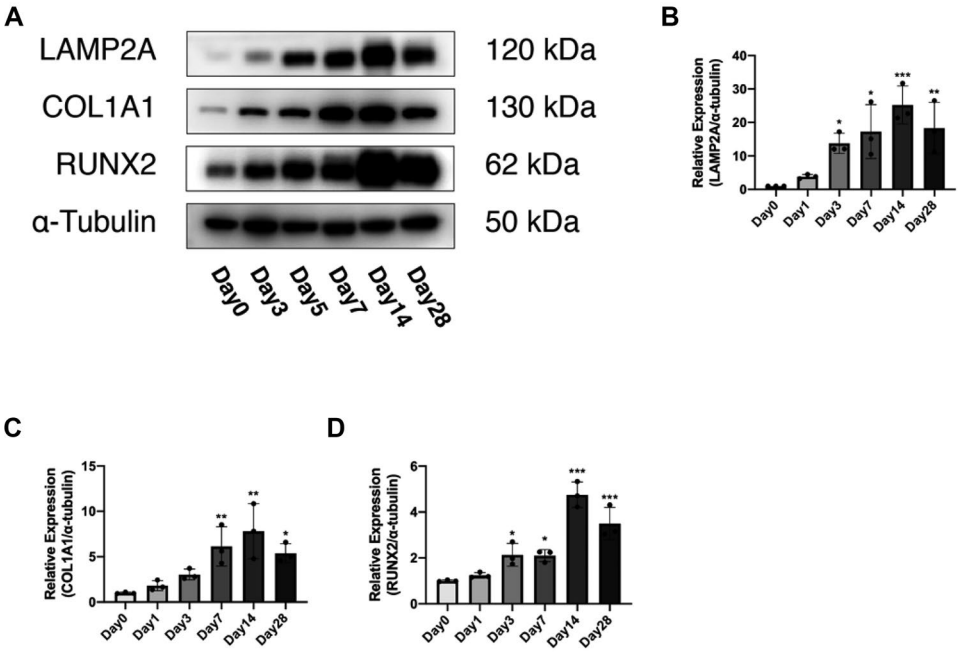

Fig. 2 Endogenous expression of LAMP2A and osteogenesis biomarkers during osteogenic differentiation and the effects of LAMP2A expression on mMSC proliferation. (**A-D**) The protein levels of LAMP2A, COL1A1, and RUNX2 (normalized to that of α-Tubulin) were determined on days 0, 3, 5, 7, 14, and 28 of osteogenic differentiation. All data are means ± SDs (n=3). $^{*}p < 0.05$, $^{**}p < 0.01$, and $^{***}p < 0.001$ versus the control group

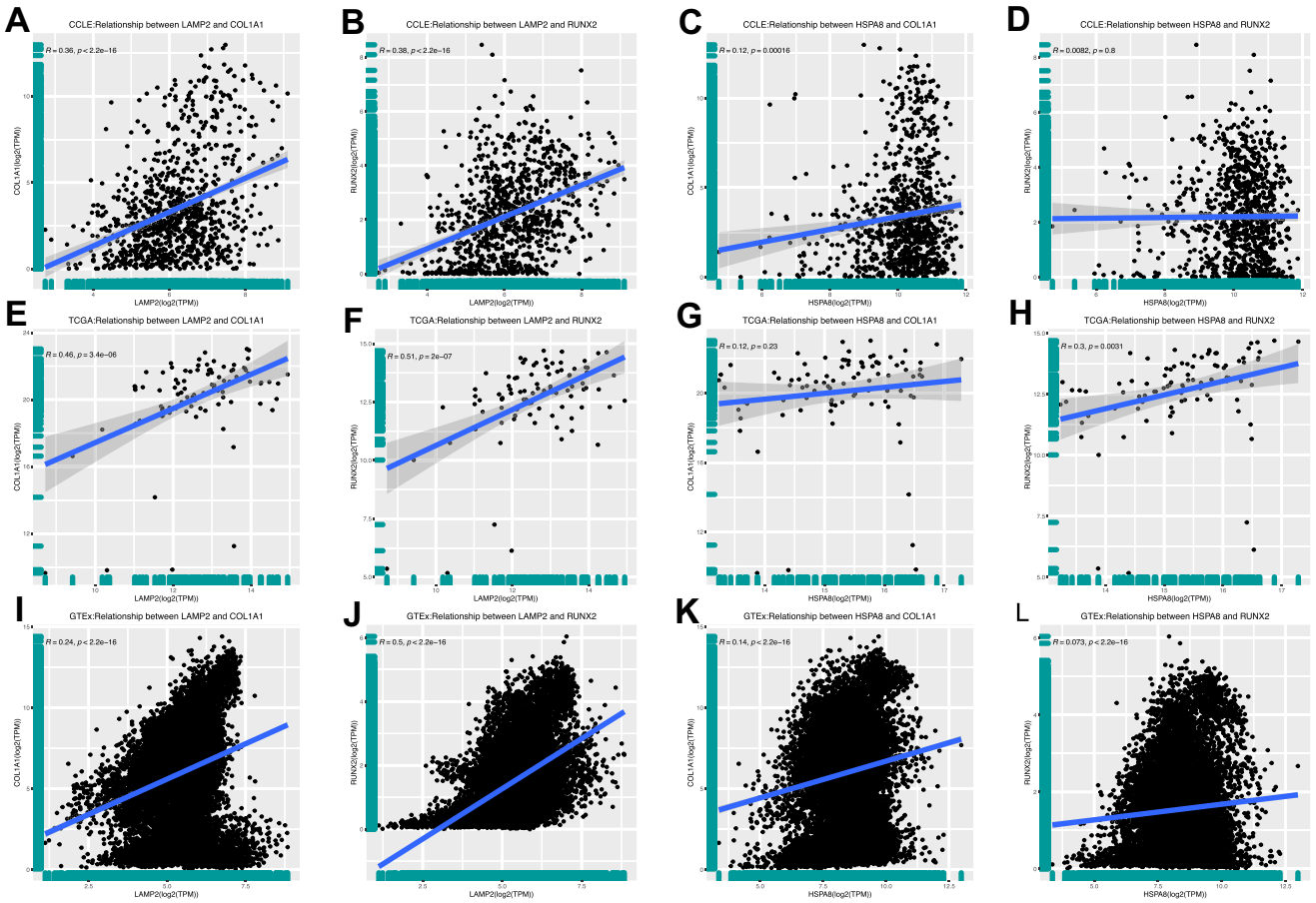

Fig. 3 Co-expression of CMA components (LAMP2A and HSPA8) and osteogenic markers. (**A**-**B**) Correlations between LAMP2, COL1A1, and RUNX2 expression levels and (**C**-**D**) correlations between HSPA8, COL1A1, and RUNX2 expression levels in the cancer cell lines of the CCLE database. (**E**-**F**) Correlations between LAMP2, COL1A1, and RUNX2 expression levels and (**G**-**H**) correlations between HSPA8, COL1A1, and RUNX2 expression levels in the osseous and chondromatous neoplasms and miscellaneous bone tumors of the TCGA database. (**I**-**J**) Correlations between LAMP2, COL1A1, and RUNX2 expression levels and (**K**-**L**) correlations between HSPA8, COL1A1, and RUNX2 expression levels in the normal tissues of the GTEx database. The correlation coefficients (R values) and the p-values are those of the Pearson correlation

of the Genotype Tissue Expression (GTEx) project, positive correlations were found between the levels of LAMP2 and both COL1A1 ($R = 0.24$, $p < 0.001$) and RUNX2 ($R = 0.50$, $p < 0.001$), as well as between the levels of HSPA8 and COL1A1 ($R = 0.14$, $p < 0.001$) and RUNX2 ($R = 0.07$, $p < 0.001$) (Fig. 3I-L). The correlations suggest that CMA components are probably related to osteogenesis.

First, we used an adenovirus system to establish mMSC LAMP2A knockdown (LA-KD) and LAMP2A-overexpressing (LA-OE) cell lines and we performed qPCR to examine the mRNA expression for 3 isoforms of Lamp2 (Lamp2a, Lamp2b and Lamp2c) (Supplementary Fig. S1). The expression of Lamp2a was significant knockdown (LA-KD) or overexpression (LA-OE) and the expression of Lamp2b and Lamp2c were not altered. Next, we used the CCK-8 assay to investigate the effects of LAMP2A knockdown or overexpression on mMSC proliferation; LAMP2A modulation had no significant effect (Fig. 4A). Western blotting revealed that LAMP2A knockdown (LA-KD) decreased COL1A1 and RUNX2 expression compared to the control group (LA-NC). By contrast, LAMP2A overexpression (LA-OE) significantly promoted the expression of osteospecific proteins (Fig. 4B-E). We performed alkaline phosphate (ALP) staining to assess early osteogenesis (day 7) and Alizarin Red S (ARS) staining to assess calcium deposition in late osteogenesis (day 21). On day 7, LAMP2A depletion significantly decreased ALP activity and LAMP2A overexpression increased ALP activity. ARS staining showed that, on day 21, calcium deposition was considerably decreased by LAMP2A depletion and increased by LAMP2A overexpression (Fig. 4I-K).

Furthermore, we explored mMSC adipogenesis via Western blotting and Oil Red O staining. Compared to the control group, the levels of adipogenesis proteins (PPARγ and C/EBPα) were inversely proportional to the LAMP2A

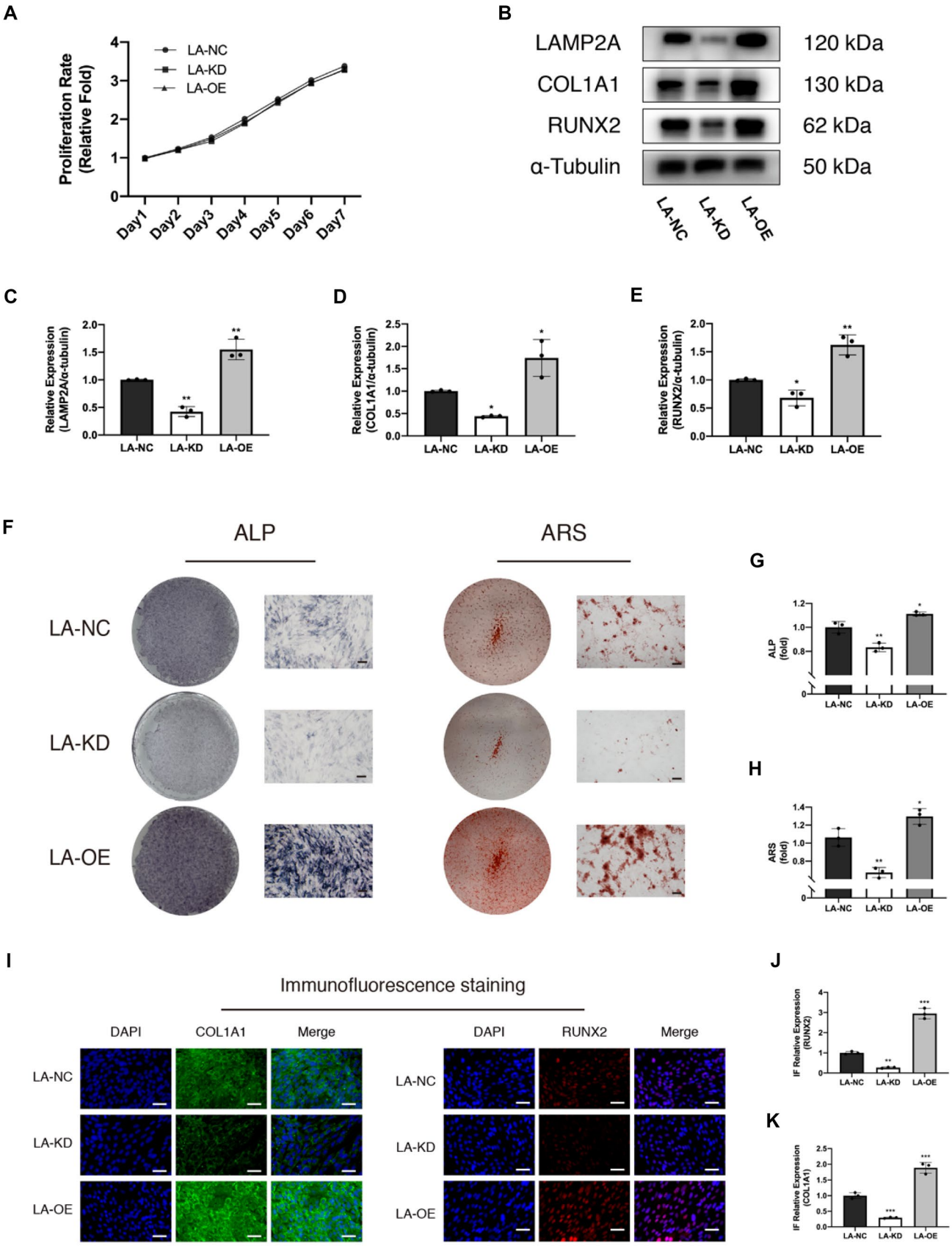
A
Proliferation Rate (Relative Fold)
LA-NC
LA-KD
LA-OE
Day1
Day2
Day3
Day4
Day5
Day6
Day7
B
LAMP2A
COL1A1
RUNX2
α-Tubulin
120 kDa
130 kDa
62 kDa
50 kDa
LA-NC
LA-KD
LA-OE
C
Relative Expression (LAMP2A/α-tubulin)
D
Relative Expression (COL1A1/α-tubulin)
E
Relative Expression (RUNX2/α-tubulin)
F
ALP
ARS
G
ALP (fold)
H
ARS (fold)
I
Immunofluorescence staining
DAPI
COL1A1
Merge
RUNX2
J
IF Relative Expression (RUNX2)
K
IF Relative Expression (COL1A1)

◂**Fig. 4** LAMP2A knockdown and overexpression respectively decrease and enhance mMSC osteogenesis. (**A**) The CCK-8 assay revealed that mMSC proliferation was not affected by LAMP2A knockdown (LA-KD) or overexpression (LA-OE). (**B**-**E**) The protein expression levels (normalized to that of α-Tubulin) of COL1A1 and RUNX2 in LA-KD and LA-OE mMSCs after 7 days of osteogenesis. (**F**-**H**) Knockdown and overexpression of LAMP2A significantly affect mMSC ALP activity (after 7 days of osteogenesis) and mineralization (after 21 days of osteogenesis). Alizarin Red S staining reveals calcium deposits. Scale bars = 100 μm. (**I**-**K**) IF staining for COL1A1 and RUNX2 after 7 days of osteogenic differentiation. Scale bars = 50 μm. All data are means ± SDs (n=3). $^{*}p < 0.05$, $^{**}p < 0.01$, and $^{***}p < 0.001$ versus the control group

level (Fig. 5A-C). Lipid droplet numbers were higher in LA-KD mMSCs and lower in LA-OE mMSCs compared to control mMSCs (Fig. 5D-E).

LAMP2A regulates the mMSC adipo-osteogenesis balance via Wnt/β-catenin/GSK3β signaling

Wnt/β-catenin/GSK3β signaling plays important roles in bone formation. We hypothesized that the effects of LAMP2A on osteogenesis would be mediated via such signaling. We analyzed the potential correlations between the levels of LAMP2A and HSPA8, and WNT3 and GSK3β, in the CCLE, TCGA, and GTEx databases (Supplementary Table 3). LAMP2A levels correlated positively with both the WNT3 ($R = 0.12$, $p < 0.001$) and GSK3β ($R = 0.30$, $p < 0.001$) levels in the 968 cancer cell lines of the CCLE database (Fig. 6A-B). The HSPA8 levels correlated moderately (positively) with the WNT3 ($R = 0.08$, $p = 0.014$) and GSK3β ($R = 0.28$, $p < 0.001$) levels (Fig. 6C-D). In the 93 osseous and chondromatous neoplasms and miscellaneous bone tumors of the TCGA database, strong correlations were evident between the LAMP2A levels and those of WNT3 ($R = 0.37$, $p < 0.001$) and GSK3β ($R = 0.58$, $p < 0.001$) (Fig. 6E-F). The correlations between the HSPA8 and WNT3 ($R = 0.40$, $p < 0.001$) and GSK3β ($R = 0.72$, $p < 0.001$) levels were also strong and positive (Fig. 6G-H). In the 17,382 normal tissues of the GTEx database, the LAMP2A levels correlated positively with the WNT3 ($R = 0.09$, $p < 0.001$) and GSK3β ($R = 0.50$, $p < 0.001$) levels (I-J). The HSPA8 levels correlated positively with those of GSK3β ($R = 0.39$, $p < 0.001$) but negatively with those of WNT3 ($R = -0.18$, $p < 0.001$) (Fig. 6K-L).

Consistent with these correlations, Western blotting revealed that the non-phosphorylated (active) β-catenin/total β-catenin ratio decreased in the LA-KD group and increased in the LA-OE group (compared to the control group) during mMSC osteogenesis. Moreover, the phospho-GSK3β(Ser9)/GSK3β level decreased with LAMP2A deletion and increased with LAMP2A overexpression (Fig. 6M-O). Moreover, a Wnt inhibitor DKK1 was used to confirm the activation of Wnt/β-catenin/GSK3β signaling by LAMP2A overexpression. With the treatment of DKK1 (500ng/ml), the promotion of Wnt/β-catenin/GSK3β signaling protein and osteogenesis marker protein by LAMP2A overexpression on day 7 were abrogated, showing by WB (Fig. 7A-B). Immunofluorescence revealed that the increase of COL1A1 and RUNX2 in mMSCs were inhibited by DKK1 on day 7 (Fig. 7C). Taken together, LAMP2A regulates the mMSC adipo-osteogenesis balance probably via Wnt/β-catenin/GSK3β signaling.

LAMP2A-overexpressing mMSCs promote healing of tibial fractures in mice

To explore the role played by CMA *in vivo*, we created a mouse model of tibial fracture and injected LA-NC and LA-OE mMSCs locally. To quantify bone healing, we subjected day-28 samples to microcomputed tomography (microCT). The BV, BV/TV and Tb.Th was increased and the Tb.Sp was decreased by injection LA-OE mMSCs locally (Fig. 8A-B) comparing with the BLANK group and LA-NC group. Immunohistochemistry (IHC) revealed that specimens treated with LA-OE mMSCs exhibited increased expression of osteopontin (OPN) in the (healing) fracture area than did BLANK and LA-NC specimens (Fig. 8C). Hematoxylin and Eosin (H&E), Safranin O/Fast Green, and Masson's Trichrome staining were used to assess remodeling of the mineralized callus. The LA-OE group exhibited a significantly smaller cortical defect (a gap) than did the control group (Fig. 8D). Moreover, histological immunofluorescence indicated that LA-OE group showed more ALP expression at the bone healing area (Fig. 9). Taking these together, LAMP2A overexpression show a promotion of the fracture healing.

Discussion

In this study, we demonstrated that LAMP2A overexpression favors osteogenesis rather than adipogenesis in mMSCs. Conversely, knockdown of LAMP2A facilitate the of adipogenesis mMSCs, whereas inhibit the osteogenesis. As for the mechanism, these results showed the activation/elimination of Wnt/β-catenin/GSK3β may involve in these processes.

Autophagy is an important biological process that protects cells from harmful external stimuli. CMA is important for bone development, and inhibition of its activity impairs bone formation [23]. It sustains hematopoietic stem cell function and the pluripotency of embryonic stem cells [31, 32], suggesting an essential role in regulation of stem cell metabolism. In 17IIA11, ST2, and MC3T3-E1 osteogenic cell lines, LAMP1 and LAMP2A could be detected at matrix vesicles only when cells stimulated with osteogenic factors [22]. In *Drosophila*, LAMP1 absence increases the levels

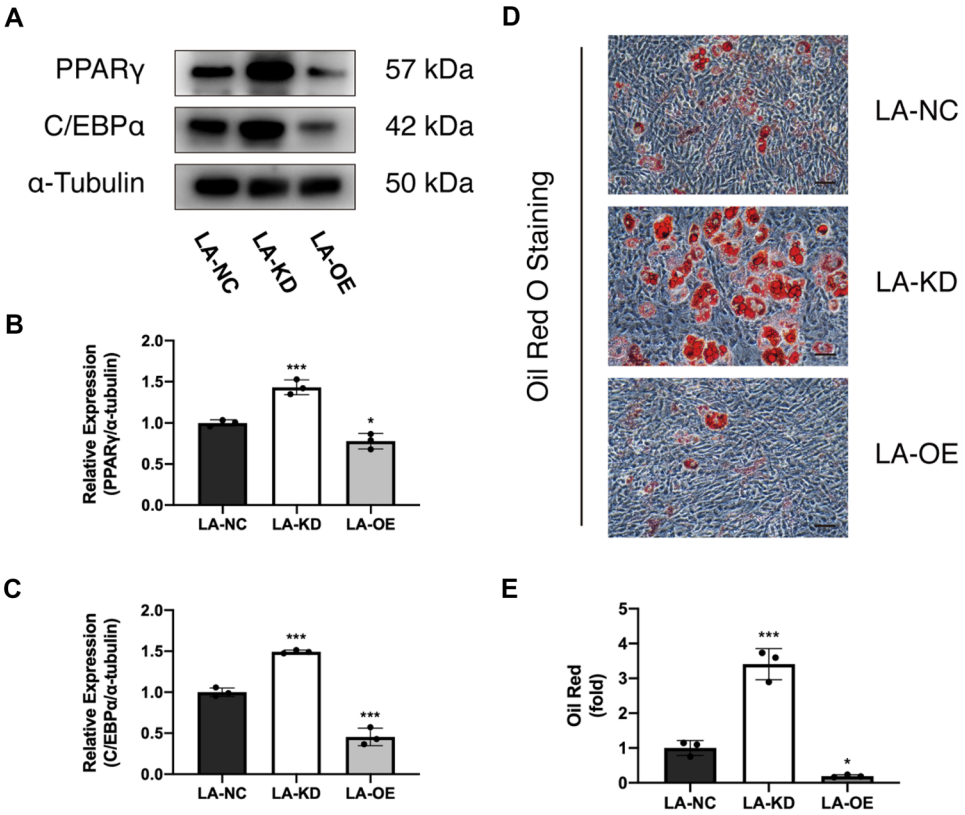

Fig. 5 LAMP2A negatively regulates mMSC adipogenesis *in vitro*. (**A**-**C**) Western blotting revealed that LAMP2A suppressed the levels of markers of adipogenic differentiation (PPARγ and C/EBPα). (**D**-**E**) Oil Red O Staining showed that LAMP2A inhibited adipogenesis. Scale bars = 100 μm. All data are means ± SDs (n=3). $^{*}p < 0.05$, $^{**}p < 0.01$, and $^{***}p < 0.001$ versus the control group

of sterols and diacylglycerols (DAGs) (important components of lipid metabolism) [33]. LAMP1 is high expression at adipocyte precursor cells but low expression at osteoblast precursor cells. However, knockdown of LAMP1 in human adipose tissue derived stem cells slightly promoted adipogenesis and had no influence on osteogenesis [34]. These results indicated that LAMP1 might be a marker to distinguish between adipocyte precursor cells and osteoblast precursor cells.

Undergoing alternative splicing, pre-Lamp2 mRNA generated three different mature mRNA encoding three different LAMP2 isoforms (LAMP2A, LAMP2B and LAMP2C) [35–37]. Despite the similarity between three LAMP2 isoforms, LAMP2B and LAMP2C do not participated in CMA in rat liver and fibroblasts [14]. LAMP2A and LAMP2B were reported as CMA regulator and macroautophagy regulator repectively [38]. Danon disease is an autophagic vacuolar myopathy caused by loss-of-function mutations in the Lamp2 gene. Recent study indicated that LAMP2B control the fusion between autophagosomes and endosomes/lysosomes via interacting with ATG14 and VAMP8. Deficiency of LAMP2B caused defects in autophagy by disrupting the STX17-independent autophagosome–lysosome fusion in human cardiomyocytes, leading to Danon disease [39]. Moreover, systemic injection of LAMP2B-AAV9 reverses multiorgan dysfunction in Lamp2-KO mice [40]. LAMP2C was revealed as a negative regulator of CMA that disrupted molecular translocation into lysosomes but did not alter macroautophagy in B cells [41]. However, in melanoma cells, LAMP2C not only manipulates CMA, but also macroautophagy [42]. LAMP2A impairment by nonsteroidal anti-inflammatory drugs (NSAIDs) induces lipid accumulation in mouse hepatocytes [43]. Furthermore, the accumulation of vertebral cancellous bone mass in young mice is reduced by LAMP2A knockout [23]. Recent study reported that Van-Gogh-like 2 (Vangl2) directly binds to LAMP2A and targets it for degradation. The Vangl2/LAMP2A ratio correlates inversely with the capacity of MSCs osteogenesis[44]. In this study, we found that LAMP2A was upregulated during mMSC osteogenic differentiation and it promoted mMSC osteogenesis and inhibited adipogenesis.

Runx2 is a key transcription factor of mMSC osteogenesis, whereas PPARγ and C/EBPα are required for adipogenesis [45, 46]. We found that LAMP2A knockdown inhibited the expression of osteogenesis-related proteins including COL1A1 and RUNX2, and enhanced the expression of the adipogenesis-related proteins PPARγ and C/EBPα; LAMP2A overexpression inhibited PPARγ and C/EBPα expression and promoted MSC osteogenic differentiation. Previous studies indicated that PPARγ (the principal transcription factor of adipogenesis) suppresses MSC osteogenic differentiation and thus contributes to osteoporosis progression [47]. MSCs exhibit a bias toward adipogenesis in the bone disorders of aging [48]. We

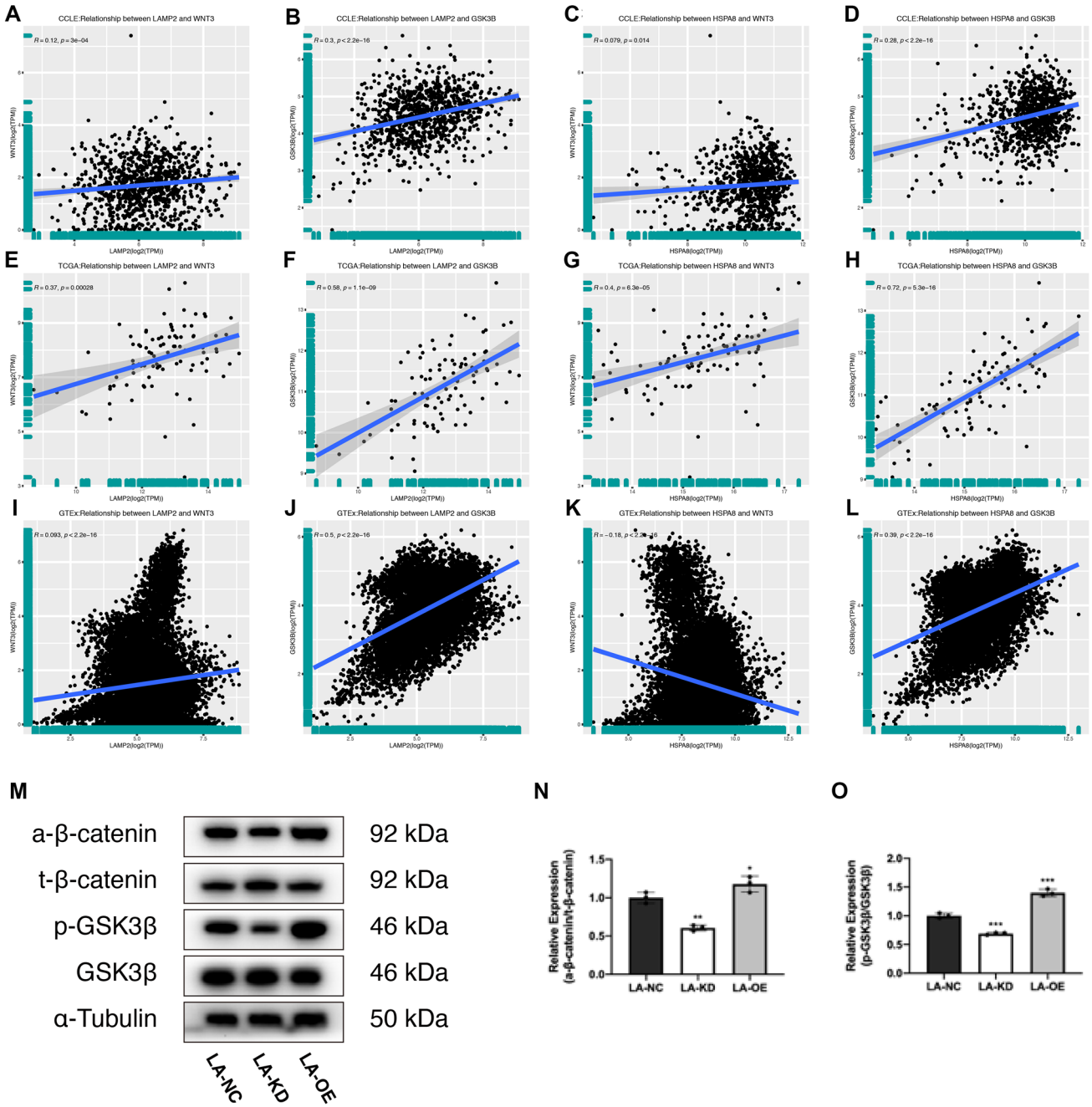

Fig. 6 LAMP2A activates the WNT/β-catenin/GSK3β pathway (**A**-**L**) Co-expression of CMA components (LAMP2A and HSPA8) and WNT/β-catenin/GSK3β pathway markers. (**A**–**B**) Correlations between the levels of LAMP2, GSK3β, and HSPA8 and (**C**-**D**) between the levels of HSPA8, WNT3, and GSK3β in the cancer cell lines of the CCLE database. (**E**-**F**) Correlations between LAMP2, WNT3, and GSK3β levels and (**G**-**H**) correlations between HSPA8, WNT3, and GSK3β levels in the osseous and chondromatous neoplasms and miscellaneous bone tumors of the TCGA database. (**I**-**J**) Correlations between the LAMP2, WNT3, and GSK3β levels and (**K**-**L**) correlations between the HSPA8, WNT3, and GSK3β levels in the normal tissues of the GTEx database. The correlation coefficients (R values) and the p-values are those of the Pearson correlation. (**M**-**O**) Western blotting reveals that LAMP2A activates the mMSC WNT/β-catenin/GSK3β pathway during osteogenesis. All data are means ± SDs (n=3). $^{*}p < 0.05$, $^{**}p < 0.01$, and $^{***}p < 0.001$ versus the control group

found that LAMP2A regulated the expression of COL1A1, RUNX2, PPARγ, and C/EBPα, reflecting the delicate balance of adipo-osteogenesis.

Many signaling pathways regulate MSC adipo-osteogenesis. The Wnt/β-catenin and p38 mitogen-activated protein kinase (MAPK) pathways promote MSC osteogenic differentiation;

the Hedgehog (Hh), Notch, and Wnt/β-catenin pathways inhibit adipogenesis [49–53]. Glycogen synthase kinase 3 (GSK3), first identified in 1980 [54], features two isoforms: α (51 kDa) and β (47 kDa). It plays central roles in various signaling pathways, including the Wnt/β-catenin, Hedgehog, and G protein-coupled ligand pathways. In mammalian cells, phosphorylation of serine 9 in the GSK3β N-terminus eliminates enzyme activity. Active GSK3β phosphorylates β-catenin, triggering β-catenin destabilization and degradation [54, 55]. Cytoplasmic accumulation of β-catenin triggers nuclear translocation of it, followed by effects on downstream gene transcription [56, 57]. We suggest that LAMP2A might promote osteogenesis by promoting phosphorylation of serine 9 of GSK3β, which decreases its activity. Then, accumulated non-phosphorylated β-catenin translocates to the nucleus and activates osteogenesis genes such as Runx2. Adipogenesis is the opposite of osteogenesis, and is negatively regulated by Wnt/β-catenin/GSK3β signaling [58–60].

We suggest that LAMP2A might suppress adipogenesis via this pathway.

Fig. 8 LAMP2A promotes bone healing *in vivo*. (**A**-**B**) Micro-CT ▶ indicates that LAMP2A promotes bone healing *in vivo*. (**A**) In the mouse model of tibial fracture, LAMP2A overexpression promoted fracture union. (**B**) LAMP2A overexpression increased the BV, BV/TV and Tb.Th, and decreased the Tb.Sp (n = 5). ns = no significance, $^{*}p < 0.05$, $^{**}p < 0.01$, and $^{***}p < 0.001$ versus the control group. The arrows indicate the fracture area. (**C**) IHC detecting osteopontin in the area of fracture healing. Arrows: OPN-positive cells. Scale bars = 50 μm. (**D**) Histological analysis of fracture healing *in vivo*. Hematoxylin and Eosin (H&E), Safranin O/Fast Green, and Masson's Trichrome staining. Scale bars = 200 μm

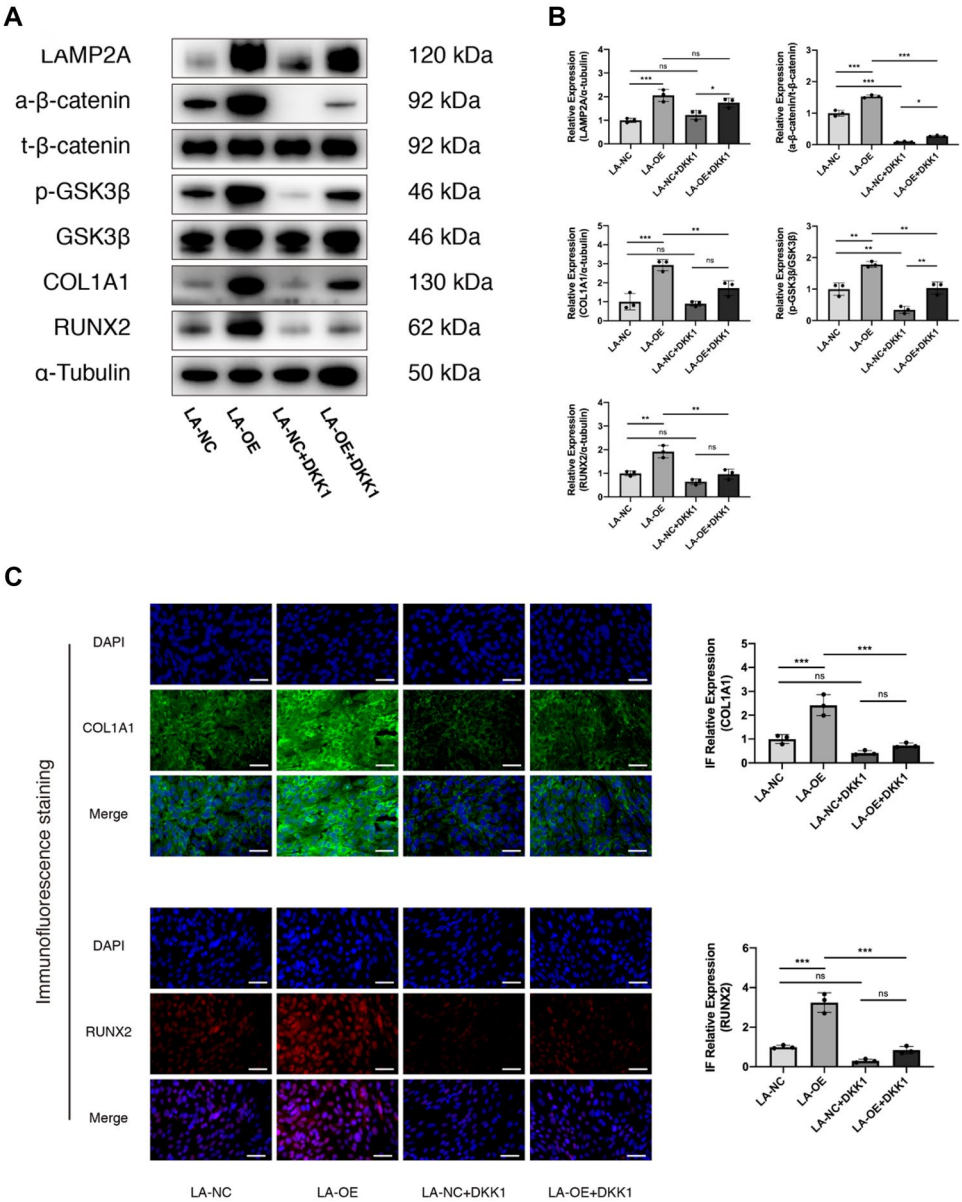

Fig. 7 DKK1 blocks the promotion of osteogenesis in LAMP2A overexpression mMSC. (**A**-**B**) Western blot reveals that the activation of WNT/β-catenin/GSK3β pathway and the promotion of osteogenesis marker (COL1A1 and RUNX2) were blocks by DKK1. (**C**) IF staining for COL1A1 and RUNX2 expression. Scale bars = 50 μm. All data are means ± SDs (n=3). ns = no significance, $^{*}p < 0.05$, $^{**}p < 0.01$, and $^{***}p < 0.001$ versus the control group

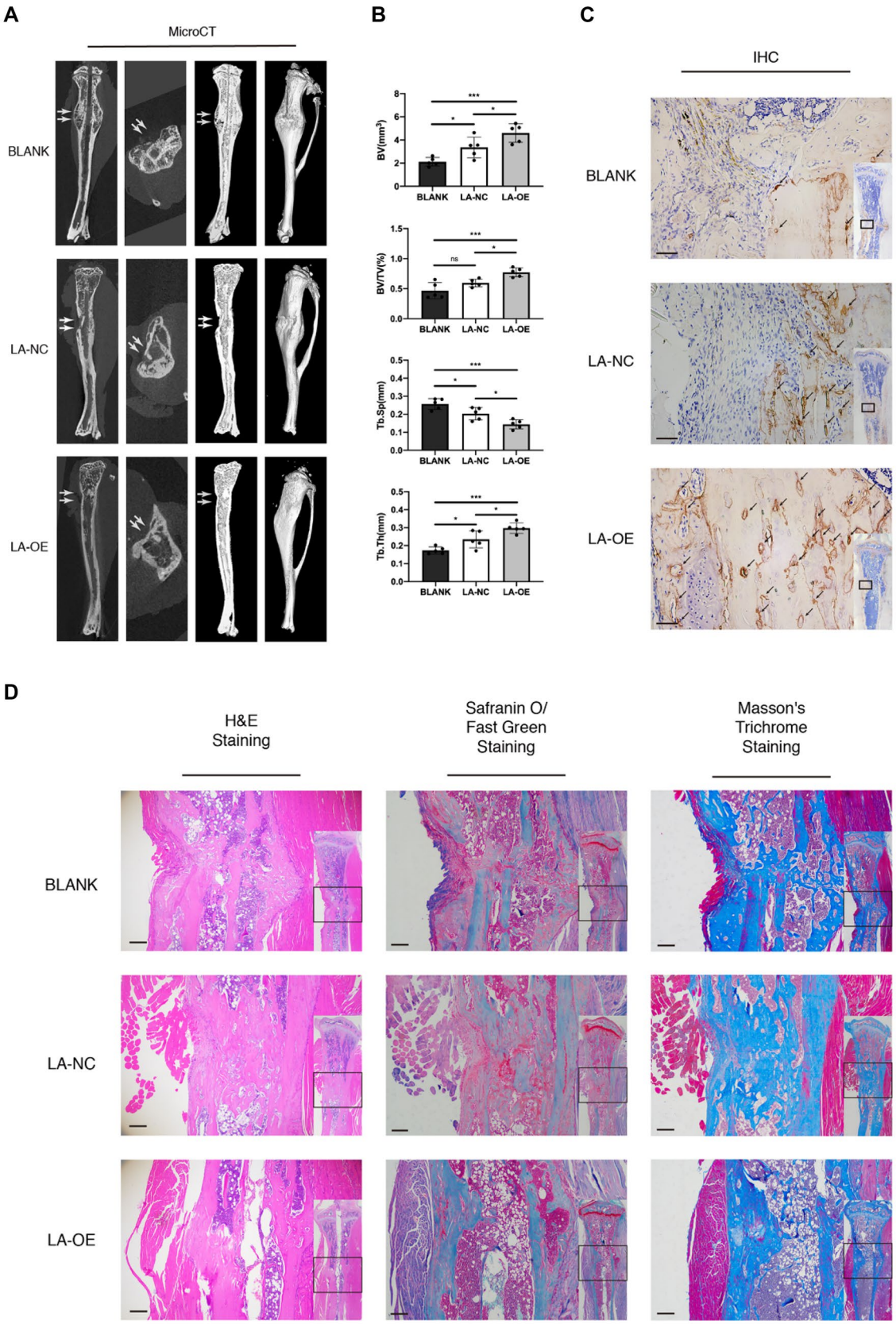
A
MicroCT
BLANK
LA-NC
LA-OE
B
BV(mm³)
BV/TV(%)
Tb.Sp(mm)
Tb.Th(mm)
BLANK
LA-NC
LA-OE
ns
C
IHC
BLANK
LA-NC
LA-OE
D
H&E Staining
Safranin O/ Fast Green Staining
Masson's Trichrome Staining
BLANK
LA-NC
LA-OE

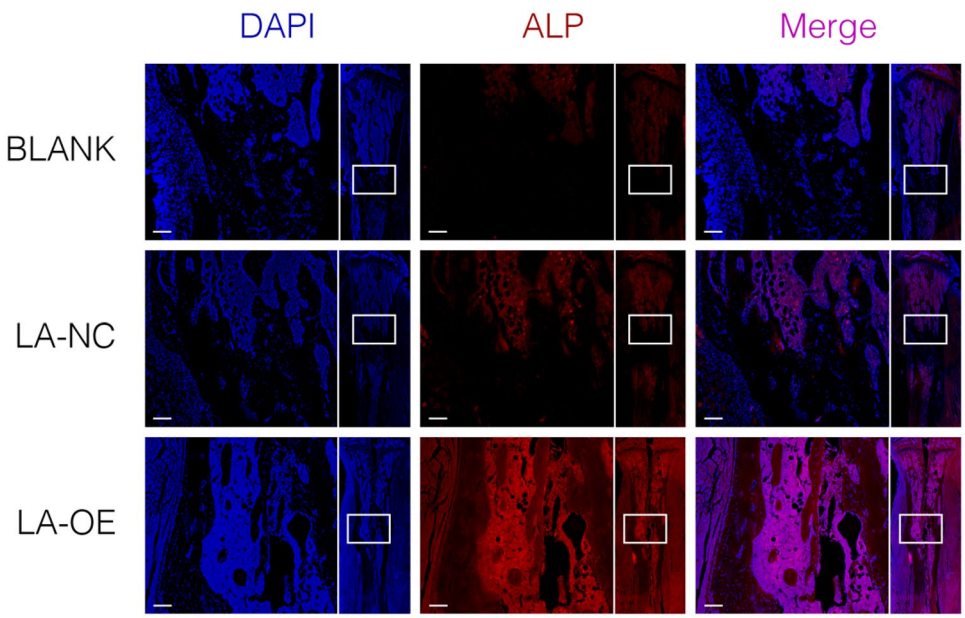

Fig. 9 LAMP2A enhanced the ALP expression at the bone healing area *in vivo*. IF show ALP was increased at the bone healing area on LA-OE group. Scale bars = 100 μm

Our work had certain limitations. First, three different isoforms of Lamp2 have different roles. Thus, the bioinformatic analysis need to be performed specifically for Lamp2a isoform. However, due to the lacking of different isoforms details in databases we used, we can only analyze the expression of Lamp2 on bioinformatic analysis. Second, LAMP2A is a lysosomal transmembrane protein involved in CMA. No evidence shows that LAMP2A has a kinase activity. Therefore, in this study, we suggest that LAMP2A promote the phosphorylation of GSK3β is a secondary effect. The direct mechanism is still unclear and need further research. Third, we used LAMP2A-knockdown or LAMP2A-overexpressing mMSCs to explore the effect of CMA on adipo-osteogenic differentiation; we did not develop CMA gene-edited animals. Such animals would be useful.

Conclusion

LAMP2A enhances the osteogenesis and suppresses the adipogenesis in the adipo-osteogenesis balance of mMSCs (Fig. 10). The mechanism of promoting osteogenesis probably via Wnt/β-catenin/GSK3β signaling pathway. LAMP2A effectively promotes healing of tibial fractures in mice.

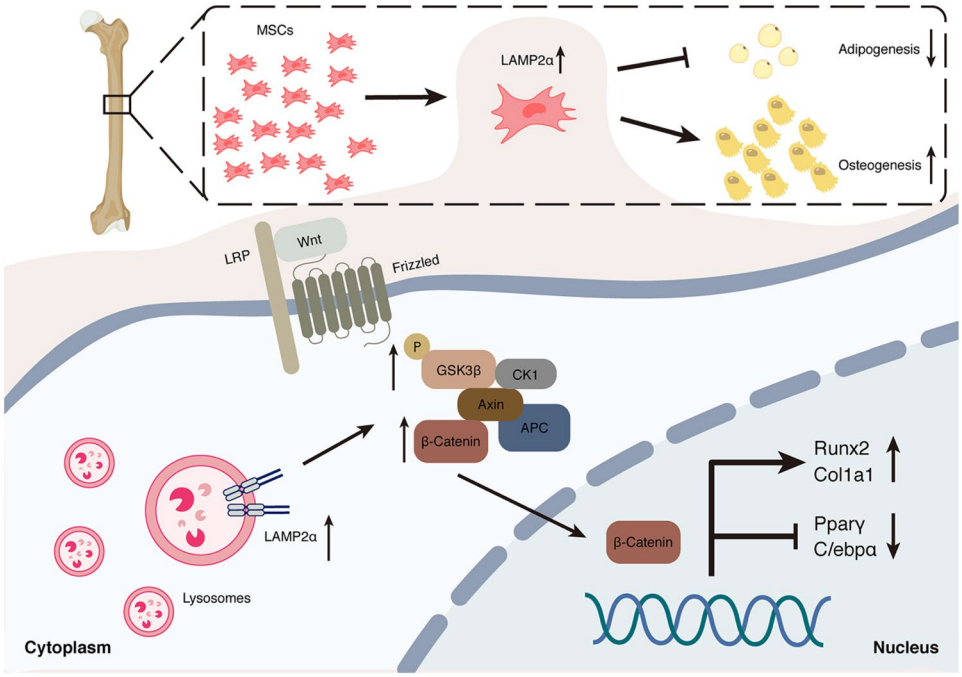

Fig. 10 CMA enhances mMSC osteogenesis and suppresses adipogenesis, probably via Wnt/β-catenin/GSK3β signaling

Abbreviations BMSCs: bone marrow mesenchymal stem cells; mMSCs: mouse bone marrow mesenchymal stem cells; GEO: Gene Expression Omnibus; DEGs: differentially expressed genes; KEGG: Kyoto Encyclopedia of Genes and Genomes; GO: Gene Ontology; BP: biological process; CCLE: the Cancer Cell Line Encyclopedia project; TCGA: The Cancer Genome Atlas project; GTEx: the Genotype Tissue Expression project; IHC: immunohistochemistry; ALP: alkaline phosphatase; ARS: alizarin red staining; CMA: chaperone-mediated autophagy; LAMP2A: lysosome-associated membrane protein type 2A; HSPA8: heat shock protein A8; COL1A1: collagen type I alpha 1 chain; RUNX2: runt-related transcription factor 2; OPN: osteopontin; PPARγ: peroxisome proliferator-activated receptor gamma; C/EBPα: CCAAT enhancer binding protein alpha; WNT3: wnt family member 3; GSK3β: glycogen synthase kinase 3 beta

Supplementary Information The online version contains supplementary material available at https://doi.org/10.1007/s00109-023-02328-1.

Acknowledgements We thank the clients who have offered assistance to this study from Clinical Research Center of the second affiliated hospital, Zhejiang university, including Xing Zhang, Meirong Yu, Sicong Chen, Liya Lin, Yunlu Chen, et al. We also appreciate the general help of Linlin Zhang and Shoumin Feng from Orthopedics Research Institute of Zhejiang University.

Authors' contributions XG, DTX and ZJP designed the research; YBW, KH and LY performed the *in vitro* experiments; YBW, KH, XYW, WJZ, LJL and JWB performed the *in vivo* experiments; YBW and HK analyzed the data; YBW, KH and XYW wrote the paper; DTX and ZJP revised the paper. All authors have read and approved the manuscript.

Funding This work was supported by grants from the National Natural Science Foundation of China (No. 81874007; 82172404) and the Natural Science Foundation of Zhejiang Province (Y21H070011).

Data availability statement The gene expression databases of mice wildtype and RUNX2 knockout humeri (GSE4911-GPL83), human non-union skeletal fracture samples and normal samples (GSE494-GPL92) were downloaded from Gene Expression Omnibus (GEO) datasets. The raw expression data of LAMP2, HSPA8, COL1A1, RUNX2, WNT3 and GSK3B genes were downloaded from the Cancer Cell Line Encyclopedia (CCLE) project (https://portals.broadinstitute.org/ccle), The Cancer Genome Atlas (TCGA) project (http://cancergenome.nih.gov/) and the Genotype Tissue Expression (GTEx) project (https://www.gtexportal.org/).

Declarations

Ethics approval and consent to participate All animal experiments were in accordance to the Animal Care and Use Committee guidelines of Zhejiang University. All experimental procedures were in accordance with the and Institutional Animal Care Use Committee at the Second Affiliated Hospital, School of Medicine, Zhejiang University.

Consent for publication Not applicable.

Competing interests The authors declare no conflicts of interest.

References

1. Rui P, Kang K (2017) National Hospital Ambulatory Medical Care Survey: 2017 emergency department summary tables. Natl Ambul Med Care Surv 37
2. Zura R, Xiong Z, Einhorn T et al (2016) Epidemiology of Fracture Nonunion in 18 Human Bones. JAMA Surg 151:e162775. https://doi.org/10.1001/jamasurg.2016.2775
3. Hak DJ, Fitzpatrick D, Bishop JA et al (2014) Delayed union and nonunions: Epidemiology, clinical issues, and financial aspects. Injury 45:S3–S7. https://doi.org/10.1016/j.injury.2014.04.002
4. Pajarinen J, Lin T, Gibon E et al (2019) Mesenchymal stem cell-macrophage crosstalk and bone healing. Biomaterials 196:80–89. https://doi.org/10.1016/j.biomaterials.2017.12.025
5. Polimeni G, Xiropaidis AV, Wikesjö UME (2006) Biology and principles of periodontal wound healing/regeneration. Periodontol 2000 41:30–47. https://doi.org/10.1111/j.1600-0757.2006.00157.x
6. Wu AC, Raggatt LJ, Alexander KA, Pettit AR (2013) Unraveling macrophage contributions to bone repair. Bonekey Rep 2:373. https://doi.org/10.1038/bonekey.2013.107
7. Wang Y, Liu Y, Chen E, Pan Z (2020) The role of mitochondrial dysfunction in mesenchymal stem cell senescence. Cell Tissue Res 382:457–462. https://doi.org/10.1007/s00441-020-03272-z
8. Pei L, Tontonoz P (2004) Fat's loss is bone's gain. J Clin Invest 113:805–6. https://doi.org/10.1172/JCI21311
9. Picke A-K, Campbell GM, Blüher M et al (2018) Thy-1 (CD90) promotes bone formation and protects against obesity. Sci Transl Med 10. https://doi.org/10.1126/scitranslmed.aao6806
10. Horwitz EM, Prockop DJ, Fitzpatrick LA et al (1999) Transplantability and therapeutic effects of bone marrow-derived mesenchymal cells in children with osteogenesis imperfecta. Nat Med 5:309–13. https://doi.org/10.1038/6529
11. Kaushik S, Massey AC, Cuervo AM (2006) Lysosome membrane lipid microdomains: novel regulators of chaperone-mediated autophagy. EMBO J 25:3921–33. https://doi.org/10.1038/sj.emboj.7601283
12. Kaushik S, Cuervo AM (2012) Chaperone-mediated autophagy: a unique way to enter the lysosome world. Trends Cell Biol 22:407–17. https://doi.org/10.1016/j.tcb.2012.05.006
13. Cuervo AM, Wong E (2014) Chaperone-mediated autophagy: Roles in disease and aging. Cell Res 24:92–104. https://doi.org/10.1038/cr.2013.153
14. Cuervo AM, Dice JF (2000) Unique properties of lamp2a compared to other lamp2 isoforms. J Cell Sci 113(Pt 24):4441–50. https://doi.org/10.1242/jcs.113.24.4441
15. Cuervo AM, Dice JF (2000) Regulation of lamp2a levels in the lysosomal membrane. Traffic 1:570–83. https://doi.org/10.1034/j.1600-0854.2000.010707.x
16. Notomi S, Ishihara K, Efstathiou NE et al (2019) Genetic LAMP2 deficiency accelerates the age-associated formation of basal laminar deposits in the retina. Proc Natl Acad Sci USA 116:23724–23734. https://doi.org/10.1073/pnas.1906643116
17. Murphy KE, Gysbers AM, Abbott SK et al (2015) Lysosomal-associated membrane protein 2 isoforms are differentially affected in early Parkinson's disease. Mov Disord 30:1639–1647. https://doi.org/10.1002/mds.26141
18. Endo Y, Furuta A, Nishino I (2015) Danon disease: a phenotypic expression of LAMP-2 deficiency. Acta Neuropathol 129:391–398. https://doi.org/10.1007/s00401-015-1385-4
19. Arad M, Maron BJ, Gorham JM et al (2005) Glycogen storage diseases presenting as hypertrophic cardiomyopathy. N Engl J Med 352:362–372. https://doi.org/10.1056/NEJMoa033349
20. Zhao K, Hao H, Liu J et al (2015) Bone marrow-derived mesenchymal stem cells ameliorate chronic high glucose-induced β-cell injury through modulation of autophagy. Cell Death Dis 6:e1885. https://doi.org/10.1038/cddis.2015.230
21. Jansen IDC, Tigchelaar-Gutter W, Hogervorst JMA et al (2020) LAMP-2 Is Involved in Surface Expression of RANKL of Osteoblasts In Vitro. Int J Mol Sci 21:1–17. https://doi.org/10.3390/ijms21176110
22. Chaudhary SC, Kuzynski M, Bottini M et al (2016) Phosphate induces formation of matrix vesicles during odontoblast-initiated

mineralization in vitro. Matrix Biol 52–54:284–300. https://doi.org/10.1016/j.matbio.2016.02.003
23. Akel N, MacLeod RS, Berryhill SB et al (2022) Loss of chaperone-mediated autophagy is associated with low vertebral cancellous bone mass. Sci Rep 12:3134. https://doi.org/10.1038/s41598-022-07157-9
24. Ritchie ME, Phipson B, Wu D et al (2015) limma powers differential expression analyses for RNA-sequencing and microarray studies. Nucleic Acids Res 43:e47. https://doi.org/10.1093/nar/gkv007
25. Hang K, Ye C, Xu J et al (2019) Apelin enhances the osteogenic differentiation of human bone marrow mesenchymal stem cells partly through Wnt/β-catenin signaling pathway. Stem Cell Res Ther 10:1–10. https://doi.org/10.1186/s13287-019-1286-x
26. Pajares M, Rojo AI, Arias E et al (2018) Transcription factor NFE2L2/NRF2 modulates chaperone-mediated autophagy through the regulation of LAMP2A. Autophagy 14:1310–1322. https://doi.org/10.1080/15548627.2018.1474992
27. Harry LE, Sandison A, Paleolog EM et al (2008) Comparison of the healing of open tibial fractures covered with either muscle or fasciocutaneous tissue in a murine model. J Orthop Res 26:1238–1244. https://doi.org/10.1002/jor.20649
28. Glass GE, Chan JK, Freidin A et al (2011) TNF-alpha promotes fracture repair by augmenting the recruitment and differentiation of muscle-derived stromal cells. Proc Natl Acad Sci USA 108:1585–90. https://doi.org/10.1073/pnas.1018501108
29. Bouxsein ML, Boyd SK, Christiansen BA et al (2010) Guidelines for assessment of bone microstructure in rodents using micro-computed tomography. J Bone Miner Res 25:1468–1486. https://doi.org/10.1002/jbmr.141
30. Gremse F, Stärk M, Ehling J et al (2016) Imalytics Preclinical: Interactive Analysis of Biomedical Volume Data. Theranostics 6:328–41. https://doi.org/10.7150/thno.13624
31. Dong S, Wang Q, Kao Y-R et al (2021) Chaperone-mediated autophagy sustains haematopoietic stem-cell function. Nature 591:117–123. https://doi.org/10.1038/s41586-020-03129-z
32. Xu Y, Zhang Y, García-Cañaveras JC et al (2020) Chaperone-mediated autophagy regulates the pluripotency of embryonic stem cells. Science 369:397–403. https://doi.org/10.1126/science.abb4467
33. Chaudhry N, Sica M, Surabhi S et al (2022) Lamp1 mediates lipid transport, but is dispensable for autophagy in Drosophila. Autophagy 00:1–16. https://doi.org/10.1080/15548627.2022.2038999
34. Xu J, Wang Y, Hsu C-Y et al (2020) Lysosomal protein surface expression discriminates fat- from bone-forming human mesenchymal precursor cells. Elife 9:. https://doi.org/10.7554/eLife.58990
35. Hatem CL, Gough NR, Fambrough DM (1995) Multiple mRNAs encode the avian lysosomal membrane protein LAMP-2, resulting in alternative transmembrane and cytoplasmic domains. J Cell Sci 108(Pt 5):2093–2100. https://doi.org/10.1242/jcs.108.5.2093
36. Gough NR, Hatem CL, Fambrough DM (1995) The family of LAMP-2 proteins arises by alternative splicing from a single gene: characterization of the avian LAMP-2 gene and identification of mammalian homologs of LAMP-2b and LAMP-2c. DNA Cell Biol 14:863–867. https://doi.org/10.1089/dna.1995.14.863
37. Konecki DS, Foetisch K, Zimmer KP et al (1995) An alternatively spliced form of the human lysosome-associated membrane protein-2 gene is expressed in a tissue-specific manner. Biochem Biophys Res Commun 215:757–767. https://doi.org/10.1006/bbrc.1995.2528
38. Eskelinen E-L, Cuervo AM, Taylor MRG et al (2005) Unifying nomenclature for the isoforms of the lysosomal membrane protein LAMP-2. Traffic 6:1058–1061. https://doi.org/10.1111/j.1600-0854.2005.00337.x
39. Chi C, Leonard A, Knight WE et al (2019) LAMP-2B regulates human cardiomyocyte function by mediating autophagosome–lysosome fusion. Proc Natl Acad Sci USA 116:556–565. https://doi.org/10.1073/pnas.1808618116
40. Manso AM, Hashem SI, Nelson BC et al (2020) Systemic AAV9.LAMP2B injection reverses metabolic and physiologic multiorgan dysfunction in a murine model of Danon disease. Sci Transl Med 12:1–13. https://doi.org/10.1126/scitranslmed.aax1744
41. Pérez L, McLetchie S, Gardiner GJ et al (2016) LAMP-2C Inhibits MHC Class II Presentation of Cytoplasmic Antigens by Disrupting Chaperone-Mediated Autophagy. J Immunol 196:2457–2465. https://doi.org/10.4049/jimmunol.1501476
42. Pérez L, Sinn AL, Sandusky GE et al (2018) Melanoma LAMP-2C Modulates Tumor Growth and Autophagy. Front cell Dev Biol 6:101. https://doi.org/10.3389/fcell.2018.00101
43. Lee W, Kim HY, Choi Y-J et al (2022) SNX10-mediated degradation of LAMP2A by NSAIDs inhibits chaperone-mediated autophagy and induces hepatic lipid accumulation. Theranostics 12:2351–2369. https://doi.org/10.7150/thno.70692
44. Gong Y, Li Z, Zou S et al (2021) Vangl2 limits chaperone-mediated autophagy to balance osteogenic differentiation in mesenchymal stem cells. Dev Cell 56:2103-2120.e9. https://doi.org/10.1016/j.devcel.2021.06.011
45. Augello A, De Bari C (2010) The regulation of differentiation in mesenchymal stem cells. Hum Gene Ther 21:1226–1238. https://doi.org/10.1089/hum.2010.173
46. Lefterova MI, Zhang Y, Steger DJ et al (2008) PPARγ and C/EBP factors orchestrate adipocyte biology via adjacent binding on a genome-wide scale. Genes Dev 22:2941–2952. https://doi.org/10.1101/gad.1709008
47. Moerman EJ, Teng K, Lipschitz DA, Lecka-Czernik B (2004) Aging activates adipogenic and suppresses osteogenic programs in mesenchymal marrow stroma/stem cells: The role of PPAR-γ2 transcription factor and TGF-β/BMP signaling pathways. Aging Cell 3:379–389. https://doi.org/10.1111/j.1474-9728.2004.00127.x
48. Meunier P, Aaron J, Edouard C, Vignon G (1971) Osteoporosis and the replacement of cell populations of the marrow by adipose tissue. A quantitative study of 84 iliac bone biopsies. Clin Orthop Relat Res 80:147–54. https://doi.org/10.1097/00003086-197110000-00021
49. Deng Z, Sharff KA, Tang N et al (2008) Regulation of osteogenic differentiation during skeletal development. Front Biosci 13:2001–21. https://doi.org/10.2741/2819
50. Bennett CN, Ross SE, Longo KA et al (2002) Regulation of Wnt signaling during adipogenesis. J Biol Chem 277:30998–31004. https://doi.org/10.1074/jbc.M204527200
51. Yuan Z, Li Q, Luo S et al (2016) PPARγ and Wnt Signaling in Adipogenic and Osteogenic Differentiation of Mesenchymal Stem Cells. Curr Stem Cell Res Ther 11:216–25. https://doi.org/10.2174/1574888x10666150519093429
52. Song B, Chi Y, Li X et al (2015) Inhibition of Notch Signaling Promotes the Adipogenic Differentiation of Mesenchymal Stem Cells Through Autophagy Activation and PTEN-PI3K/AKT/mTOR Pathway. Cell Physiol Biochem 36:1991–2002. https://doi.org/10.1159/000430167
53. Fontaine C, Cousin W, Plaisant M et al (2008) Hedgehog signaling alters adipocyte maturation of human mesenchymal stem cells. Stem Cells 26:1037–46. https://doi.org/10.1634/stemcells.2007-0974
54. Ding VW, Chen RH, McCormick F (2000) Differential regulation of glycogen synthase kinase 3β by insulin and Wnt signaling. J Biol Chem 275:32475–32481. https://doi.org/10.1074/jbc.M005342200
55. Wu D, Pan W (2010) GSK3: a multifaceted kinase in Wnt signaling. Trends Biochem Sci 35:161–168. https://doi.org/10.1016/j.tibs.2009.10.002
56. Hur E-M, Zhou F-Q (2010) GSK3 signalling in neural development. Nat Rev Neurosci 11:539–51. https://doi.org/10.1038/nrn2870
57. Baron R, Kneissel M (2013) WNT signaling in bone homeostasis and disease: from human mutations to treatments. Nat Med 19:179–92. https://doi.org/10.1038/nm.3074

58. Gustafson B, Smith U (2010) Activation of canonical wingless-type MMTV integration site family (Wnt) signaling in mature adipocytes increases beta-catenin levels and leads to cell dedifferentiation and insulin resistance. J Biol Chem 285:14031–41. https://doi.org/10.1074/jbc.M110.102855
59. Chen J-R, Lazarenko OP, Wu X et al (2010) Obesity reduces bone density associated with activation of PPARγ and suppression of Wnt/β-catenin in rapidly growing male rats. PLoS One 5:e13704. https://doi.org/10.1371/journal.pone.0013704
60. Reggio A, Rosina M, Palma A et al (2020) Adipogenesis of skeletal muscle fibro/adipogenic progenitors is affected by the WNT5a/GSK3/β-catenin axis. Cell Death Differ 27:2921–2941. https://doi.org/10.1038/s41418-020-0551-y